NLRC4 activation needs lncRNA *LNCGM1082*

Yunhuan Gao
Nankai University
Yazheng Yang
Nankai University https://orcid.org/0000-0003-2043-0369
Jianmei Wei
Nankai University
Jianmei Yue
Nankai University
Ya Wang
Nankai University
Qianjing Zhang
Nankai University
Mengli Jin
Nankai University
Rong Wang
Nankai University
Xiaorong Yang
Nankai University
Junqi Zhang
Nankai University
Xinqi Liu
Nankai University
Yuan Zhang
Nankai University
Rongcun Yang (ryang@nankai.edu.cn)
Nankai University https://orcid.org/0000-0002-5826-4493

Article

Keywords: Intracellular Bacteria Infection, Diverse Stimuli Sensing, Pyroptotic Cell Death, Salmonella typhimurium, PKCδ Binding

Posted Date: May 21st, 2021

DOI: https://doi.org/10.21203/rs.3.rs-474866/v1

Abstract

The activation of NLRC4 is a major host response against the infection by intracellular bacteria. However, there still remain challenges in understanding the activation upon sensing of diverse stimuli. We here found that lncRNA *LNCGM1082* plays a critical role in the activation of NLRC4. *LNCGM1082* in macrophages could affect maturation of interleukin (IL)-1β and pyroptotic cell death only after exposed to NLRC4 ligand. Similar to *NLRC4*-/- mice, *LNCGM1082*-/- mice were high sensitive to *Salmonella typhimurium* infection. *LNCGM1082* deficiency in mouse or human macrophages had reduced IL-1β maturation and pyroptosis. Mechanistically, *LNCGM1082* could induce the combination of PKCδ with NLRC4 in both mice and human. There was absence of binding of NLRC4 with PKCδ in *LNCGM1082*-/- macrophages. This lncRNA could be induced by *Salmonella typhimurium* through TLR5 in the macrophages of both mice and human. Thus, our data indicate that *LNCGM1082* induced by TLR5 can mediate the binding of PKCδ with NLRC4 to cause the activation of NLRC4.

Introduction

NLR family CARD domain containing 4 (NLRC4) inflammasomes can protect mucosal barriers such as the lung, stomach and intestine from invading bacterial pathogens such as *S Typhimurium*[1]. They exist in multiple cell types including those of hematopoietic such as monocytes, macrophages and non-hematopoietic origin such as intestinal epithelial cells[1]. NLRC4 inflammasome is a cytosolic sensor of bacteria that activates caspase-1 and initiates potent immune responses. Activation of NLRC4 inflammasomes includes trigger (e.g. cytosolic flagellin), sensor (NLR apoptosis inhibitory protein (NAIP)), nucleator (NLRC4), adaptor (apoptosis-associated speck-like protein (ASC)) and effector (caspase-1)[2]. Activated caspase-1 together with caspase-11 cleaves, and matures the cytokines IL-1β and IL-18 as well as the pore-forming protein gasdermin D (GSDMD)[3,4]. Maturation GSDMD causes pyroptotic cell death to release mature IL-1β and IL-18, leading to inflammatory responses to control infection. Pathogenic activators of the NLRC4 are mainly derived from Gram-negative bacteria namely *Salmonella, Legionella, Shigella*, and *Pseudomonas spp*. These bacteria possess flagellin, a type III (T3SS) or type IV (T4SS) secretion system rod proteins that are recognized by the NAIP proteins, constituting unique binding partners of NLRC4[5]. Activity of NLRC4 inflammasomes depends on NLRC4 activation, which not only relies on NLR family apoptosis inhibitory proteins (NAIPs) for sensing bacterial components in the cytosol [6] but also phosphorylation[7,8] and ubiquitination[9]. NLRC4 could be phosphorylated by PKCδ [6] and LRRK2[7]. They form a complex with NLRC4 in the macrophages, and the formation of the complex leads to the phosphorylation of NLRC4 at Ser533[7,8]. However, they still remain challenges in understanding the regulation of NLRC4 activation upon sensing of diverse stimuli.

The overexpression, deficiency or mutation of lncRNA genes has been implicated in numerous human diseases[10]. LncRNAs are involved in numerous important biological phenomena such as imprinting genomic loci, shaping chromosome conformation and allosterically regulating enzymatic activity[11,12]. We

here found that *LNCGM1082* can induce the binding of NLRC4 and PKCδ to cause the phosphorylation of NLRC4.

Results

LNCGM1082 **in macrophages promotes maturation of IL-1β and pyroptosis.**

While we investigated the lncRNAs in myeloid derived cells, we found that *lncRNA GM1082 (LNCGM1082)* could not only be expressed in myeloid derived suppressive cells (MDSC) [13] (Fig. 1a) but also in macrophages and dendritic cells, but not in $CD4^+$, $CD8^+$ T cells and $CD19^+$B cells (Fig. 1b). *LNCGM1082* expression in macrophages could be further confirmed using fluorescence in situ hybridization (FISH) and Northern blot (Fig. 1c, d). This *LNCGM1082* belonged to intergenic lncRNA, which was predominately localized to the cytoplasm (Fig. 1c). We next investigated the function(s) of *LNCGM1082* in macrophages. The macrophages were transfected using *LNCGM1082* shRNA or exogenous *LNCGM1082* lentiviruses, and then exposed to different Toll-like receptor ligands. Silencing and overexpressing of *LNCGM1082* had not effective effects on transcription and production of cytokines such as IL-1β, IL-6 and TNFα (Supplementary Fig. 1). However, while macrophages were primed with lipopolysaccharides (LPS) and subsequently treated with the flagellin (LPS with flagellin)[14], this *LNCGM1082* could markedly promote mature IL-1β production (Fig. 1e, f). LPS, LPS with ATP, LPS with nigericin or LPS with poly (dA and dT) did not cause significantly changes of mature IL-1β in these macrophages (Fig. 1e, f). Since matured IL-1β production often companys with pyroptosis [3,4], which is a lytic cell death induced by pathogen infection or endogenous challenge[15]. We also investigated the pyroptosis in the *LNCGM1082* shRNA or exogenous *LNCGM1082* transfected macrophages after exposed to LPS with flagellin. Data showed that silencing *LNCGM1082* markedly reduced pyroptosis; whereas exogenous *LNCGM1082* promoted the pyroptosis of macrophages (Fig. 1g). LPS, LPS with ATP, LPS with nigericin or LPS with poly (dA and dT) also induced pyroptosis, but no difference was found in *LNCGM1082 shRNA* or exogenous *LNCGM1082* transfected macrophages (Fig. 1g). There exist multiple pathways to induce IL-1β maturation and pyroptosis, including those primed by NLRC4, caspase-11 and NLRP3 etc.. LPS with flagellin is activator of NLRC4[2]; LPS with ATP is known as activator of caspase-1[16], which can activate caspase-11[17]; LPS with nigericin can activate NLRP3[18]; LPS with poly (dA and dT) is recognized by multiple PRRs such as cytosolic DNA sensors (CDS) including cGAS, AIM2, DAI, DDX41, IFI16, and LRRFIP1[19]. Since *LNCGM1082* transfected macrophages exhibited difference in mature IL-1β production and pyroptosis only after responded to LPS with flagellin (NLRC4 ligand) but not LPS with nigericin (NLRP3 ligand), LPS with ATP (caspase-1 ligand) or LPS with poly (dA and dT) (CDS ligand), suggesting that *LNCGM1082* mediated IL-1β and pyroptosis may be through NLRC4 but not caspase-1 or NLRC3.

LNCGM1082 **has similar effects with NLRC4 on regulating maturation of IL-1β and pyroptosis of macrophages**

To further determine function(s) of *LNCGM1082* in macrophages, we generated *LNCGM1082* deficient mice. The macrophages were isolated from wild type (wt) and *LNCGM1082-/-* mice. After exposed to LPS with flagellin (NLRC4 ligand), LPS, LPS with ATP (caspase-1 ligand), LPS with nigericin (NLRP3 ligand) or LPS with poly (dA and dT) (CDS ligand), only LPS with flagellin caused decreased mature IL-1β but not transcriptional levels of IL-1β in *LNCGM1082-/-* macrophages (Fig. 2a), further suggesting that *LNCGM1082* may affect NLRC4 mediated pathway. Thus, we next compared the *LNCGM1082-/-* macrophages with those from *NLRC4-/-* mice. Data indeed showed that similar effects of *LNCGM1082-/-* with *NLRC4-/-* on the macrophages after exposed to LPS with flagellin or *S.T* and also LPS with ATP (Fig. 2b, c), which is different from *caspase-1/11-/-* and *NLRP4-/-* macrophages. *LNCGM1082-/-* and *NLRC4-/-* macrophages had reduced IL-1β maturation after exposed to LPS with flagellin or *S.T* but not LPS with ATP (Fig. 2b, c). We also investigated the effects of *LNCGM1082* on the pyroptosis of macrophages. Similar resistance to flagellin-mediated pyroptosis between *LNCGM1082-/-* and *NLRC4-/-* macrophages could also be observed after exposed to LPS with flagellin but not LPS with ATP (Fig. 2d-e). The macrophages from *caspase-1/11-/-* and *NLRP3-/-* mice exhibited different pyroptosis from *LNCGM1082-/-* macrophages after exposed to LPS with flagellin, LPS with ATP or *S.T* (Fig. 2d, e). The other effects of *LNCGM1082* on the macrophages were further investigated through microarray. Data did not exhibit significant effects of *LNCGM1082* on the expression of genes (Fig. 2f). Taken together, all of these suggest that *LNCGM1082* may exert similar roles with NLRC4 to affect IL-1β maturation and pyroptosis on the macrophages.

Similar to NLRC4**-/- mice**, LNCGM1082**-/-mice are high sensitive to** Salmonella typhimurium **infection**

Since *LNCGM1082-/-* mice have similar effects with *NLRC4-/-* mice in regulating IL-1β maturation and pyroptosis of macrophages in response to flagellin, we employed *Salmonella typhimurium* (*S. T*) infection model, which is used to detect the role(s) of NLRC4[20], to further test the role of *LNCGM1082*. *LNCGM1082-/-*, *NLRC4-/-* and control mice were individually infused with *S.T* (200 CFUs/mouse). Then we observed the changes of body weight and survival rate. Similar to previous reports[21], *NLRC4-/-* mice had markedly reduced body weight and survival rate. *LNCGM1082-/-* mice had similar body weight changes and survival rates with *NLRC4-/-* mice (Fig. 3a, b). Bacteria can colonize and infect anatomical sites other than the gastrointestinal tract of the mammalian host, such as the lungs, liver and spleen[22–24]. Similar to *NLRC4-/-* mice[22–24], *LNCGM1082-/-* mice also succumbed to infection more quickly and had increased bacterial burden in the lung, liver and spleen compared with wt mice (Fig. 3c-e). These *LNCGM1082-/-* mice also had reduced inflammation in lung tissues, decreased IL-1β in sera and inflammatory cells (Fig. 3f-h). Meanwhile, we compared *LNCGM1082-/-* with *caspase-1/11-/-* or *NLRC3-/-* mice, both *NLRP3-/-* and *caspase-1/11-/-* mice also showed different sensitivity to *S. T* infection as compared to *LNCGM1082-/-* mice (Fig. 3a-h). Since *S.T* infection not only causes inflammation of gut epithelial cells but also gut macrophages[25,26], we transplanted bone marrow cells to irradiated recipients to demonstrate the involvement of gut macrophages. The wt mice with a *LNCGM1082-/-* bone marrow reconstitution had elevated bacterial burden in the liver, lung and spleen as compared with wt mice with wt bone marrow reconstitution (Supplementary Fig. 2), indicating that macrophages play a main role in

response to *S.T* infection. Meanwhile, we also performed LPS toxic experiments, no differences were showed in *LNCGM1082-/-* and wt mice (Supplementary Fig. 3), further indicating that there does not exist relationship between *LNCGM1082* with caspase-1[16]. In addition, enteropathogenic *Escherichia coli* also can activate NLRC4[21]. While equal amount of GFP-labeled *Escherichia coli*, which were isolated from DSS-mediated colitis and demonstrated to promote inflammation[27], both *LNCGM1082*-/- and *NLRC4*-/- mice had also similarly increased bacteria as compared to wt mice in the feces after 2 days (Fig. 3i). Taken together, similar to *NLRC4*-/- mice, *LNCGM1082*-/- mice are high sensitivity to *S.T* and *E. coli* infection.

Binding of LNCGM1082 **with NLRC4 and PKCδ to induce NLRC4 phosphorylation**

Since lncRNA may be directly through binding with proteins to exert its role [11], we detected whether this *LNCGM1082* could bind with NLRC4 to regulate NLRC4 function. We first examined NLRC4 phosphorylation in the macrophages after exposed to *S. T* or flagellin. *LNCGM1082-/-* abolished the phosphorylation of NLRC4 (Fig. 4a). NLRC4 may be phosphorylated through PKCδ or LRRK2 to form a complex with NLRC4 in the macrophages[7,8]. Immunoprecipitation (IP) showed that *LNCGM1082-/-* macrophages were no binding of NLRC4 with PKCδ, similar to *NLRC4*-/- macrophages (Fig. 4b), suggesting that *LNCGM1082* may bind with NLRC4 and PKCδ. Indeed, RNA immunoprecipitation analyses (RIP) showed that *LNCGM1082* could not only bind with NLRC4 but also PKCδ (Fig. 4c, d). These bindings were further confirmed through FISH and immunostaining of *LNCGM1082* with NLRC4 and PKCδ (Fig. 4e-f). Marked binding of NLRC4 and PKCδ was observed in wt mice; whereas there was absence of binding in the *LNCGM1082*-/- macrophages after exposed to flagellin and LPS (Fig. 4e, f). Furthermore, the binding of *LNCGM1082* with NLRC4 and PKCδ could be confirmed with increased concentration of flagellin (Supplementary Fig. 4a, b).

We next wanted to found the potential motif in *LNCGM1082*, which could be bound by NLRC4 or PKCδ. We first used iCLIP truncation track to show the positions of iCLIP cDNA truncations at *LNCGM1082* with peak height corresponding to the cDNA counts (Supplementary Fig. 5a). Then we got lncRNAs by RIP using anti-NLRC4, and digested by RNA enzymes to establish cDNA library after amplification. A potential binding motif in *LNCGM1082*, which could interact with NLRC4 by MEME algorithm analyses, was found (Supplementary Fig. 5b). We also predicted the binding site between PKCδ and *LNCGM1082* using RNAInter software (http://www.rna-society.org/raid/home.html) (Supplementary Fig. 5c). Sequence logo of PKCσ recognition motif was generated by MEME analysis of lncRNA sequence read clusters (Supplementary Fig. 5d). We named NLRC4 binding site as “D1” and PKC binding site “D2”, and constructed the mutated *LNCGM1082* plasmids which lack D1, D2 and D1 + D2 sites (Fig. 4g). RNA-pull down demonstrated that D1 fragment of *LNCGM1082* could bind with NLRC4; Whereas D2 was essential with PKCδ (Fig. 4h, i). The binding of *LNCGM1082* with NLRC4 and PKCδ also was confirmed by isothermal titration calorimetry (ITC) analyses (Fig. 4j, K). ITC also confirmed that D1 and D2 fragments were necessary in the binding of *LNCGM1082* with NLRC4 and PKCδ (Fig. 4j, K). To further confirm the binding of *LNCGM1082* with NLRC4 and PKCδ, we also cloned the NLRC4, PCK δ and their fragments

with tagged V5 (Supplementary Fig. 6a), and then cotranfected 293 T cells with *LNCGM1082*. RIP using anti-V5 antibody in cotransfected HEK293T cells also showed the binding of *LNCGM1082* with NLRC4 and PKCδ (Supplementary Fig. 6b, c). Furthermore, LRR region of NLRC4 was critical in binding of NLRC4 with *LNCGM1082* (Supplementary Fig. 6b). Since LRRK2 could also cause the activation of NLRC4, we also detected the binding of *LNCGM1082* with LRRK2[8]. Data did not show the combination between *LNCGM1082* with LRRK2 (Supplementary Fig. 7a). In addition, caspase-1, caspase-11 and NLRP3 could also regulate the production of mature IL-1β and pyroptosis, data did not show that the binding of *LNCGM1082* with caspase-1, caspase-11 and NLRP3 (Supplementary Fig. 7b-d). Taken together, *LNCGM1082* can bind with NLRC4 and PKCδ to cause the phosphorylation of NLRC4.

Similar functions of human LNCGM1082 **with mice in the macrophages**

LNCGM1082 was highly conserved between mouse and human with 43.85 % homology. NLRC4 and PKCδ were also highly conservative between human and mouse based on the DNAMAN software. We next investigated whether there also existed similar function with mice in human macrophages. We first detected the expression of *LNCGM1082* in human macrophages. Human monocyte/macrophages cells line THP-1 and macrophages in colon tissues exhibited the expression of human *LNCGM1082* (Fig. 5a). THP1 cells can recognize flagellin from *S. T*[28,29]. To determine the function(s) of *LNCGM1082* in the human macrophages, we generated the human *huLNCGM1082*-/- macrophages using CRISPR CAS9 gene knockout technique with demonstrated *huLNCGM1082* knockout (Fig. 5a). Similar effects of *LNCGM1082* deficiency on mouse macrophages were also observed in *huLNCGM1082*-/- macrophages, including the reduced IL-1β maturation and resistance to pyroptosis after exposed to flagellins with LPS or *S.T* infection (Fig. 5b-f); Whereas similar roles in the macrophages were not observed after exposed to LPS with ATP, LPS with nigericin or LPS with poly (dA + dT)(Fig. 5b-f). Thus, *huLNCGM1082* can promote IL-1β maturation and sensitivity to pyroptosis, which are similar with mouse *LNCGM1082* in the macrophages.

Human NLRC4 activation needs LNCGM1082

Since human and mouse *LNCGM1082* have similar functions in macrophages, we further analyzed two lncRNAs using bioinformatics. There existed common binding motifs in both human and mice to NLRC4 and PKCδ (Supplementary Fig. 8a). Meanwhile we also used SWISS-MODEL software to model the protein crystal structure of NLRC4 and PKCδ of human and mice. Crystal structures of NLRC4 and PKCδ in human and mice were also similar (Supplementary Fig. 8b). All of these suggest that human *LNCGM1082* may have similar binding with mice in NLRC4 and PKCδ. Indeed, marked binding of NLRC4 and PKCδ was observed in THP1; whereas there was absence of binding of NLRC4 and PKCδ in the *huLNCGM1082*-/- THP1 cells after exposed to LPS with flagellin (Fig. 6a, b), which were similar to mouse *LNCGM1082*-/- macrophages. NLRC4 phosphorylation in *huLNCGM1082*-/- macrophages was also absent after exposed to flagellin or *S.T* (Fig. 6c). *HuLNCGM1082* also exhibited the binding with NLRC4 and PKCδ using IP and RIP (Fig. 6d-f). These bindings were further confirmed by ITC (Fig. 6g). Data also confirmed that *LNCGM1082* D1 region was critical in binding with NLRC4; Whereas D2 could mediate the

binding of *LNCGM1082* with PKCδ (Fig. 6g-i). Thus, *huLNCGM1082* can also bind with NLRC4 and PKCδ in human macrophages.

TLR5 mediates the expression of LNCGM1082

Finally, we investigated what could regulate the expression of *LNCGM1082*.

While we analyzed the expression of genes in gut tissues after *S.T* infection, the expression of *LNCGM1082* was markedly increased (SupplementaryFig. 9), suggesting that *LNCGM1082* expression may be related to *S.T* infection. Thus we analysed the *LNCGM1082* expression after exposing to *S. T* or its flagellin, which is one of the key effector molecules which not only act as the cytosolic sensor but also binds and activates membrane-bound TLR5[30,31]. Data exhibited that both *S. T* and flagellin could induce the expression of *LNCGM1082* in mouse macrophages but not in *TLR5*-/- macrophages (Fig. 7a-i). TLR5 can be expressed in human THP-1 cells[32]. Furthermore, both *S. T* and flagellin induced *LNCGM1082* expression was dose- and time-dependent (Fig. 7b-d,i). Both *S. T* and flagellin also induced *LNCGM1082* expression in human macrophage THP-1 (Fig. 7j-m). Notably, this express could be rapidly detected after exposing to *S.T* (Fig. 7). Finally, we also did not found the binding of *LNCGM1082* with NLRC4 and PKCδ in TLR5-/- macrophages after exposed to LPS with flagellin (Fig. 7n). Taken together, TLR5 can induce *LNCGM1082* in both human and mouse macrophages.

Discussion

In this study we report an important physiological role for *LNCGM1082* in the host against *S. T* infection. *LNCGM1082* deficiency causes reduced mature Il-1β and pyroptosis in the macrophages. *LNCGM1082*-/- mice are high sensitivity to *S. T* infection. Mechanistically, we found that activation of NLRC4 needs *LNCGM1082*, which can bind with PKCδ and NLRC4 to cause the phosphorylation of NLRC4. We also demonstrate that *LNCGM1082* expression can be rapidly induced by *S. T* through TLR5, which may have an important significance in switching the activation of NLRC4 by *S. T* to induce inflammation to eliminate bacteria (Fig. 7o). These findings may be promising targets for designing therapeutic drugs for disease treatments and prevention.

The activation of NLRC4 is an important event during NLRC4 inflammasome activation. Biochemical, structural and genetic studies established that activation of NLRC4 requires NAIP proteins (NAIP1, NAIP2, NAIP5, and NAIP6 in C57BL/6 mice), acting as sensors to detect bacterial flagellin, T3SS needle or rod proteins[33]. NLRC4 are also transcriptionally induced by interferon regulatory factor (IRF) 8[34]. IRF8 acts as a transcriptional activator for murine NAIPs 1, 2, 5, and 6 and NLRC4. NLRC4 is also subject to posttranslational modifications that can regulate their assembly and function [7,8,9]. Earlier work in murine macrophages identified that NLRC4 was phosphorylated at position S533 by PKC-δ in response to *S. Typhimurium* [7]. Furthermore, this modification was required for NLRC4 inflammasome assembly[7]. NLRC4 S533 can interact directly with infection-induced NLRP3, which further recruits ASC and activates caspase-1[35]. Activated NLRC4 also undergoes substantial structural reorganization, interacts and

activates another quiescent NLRC4 molecule to ultimately form a 10- to 12-spoke wheel- or disk-like architecture[36,37]. Notably, the importance of PKCδ and phosphorylation at S533 in NLRC4 inflammasome activation are questioned in subsequent work. For example, leucine-rich repeat kinase 2 (LRRK2) was also shown to phosphorylate NLRC4 aS533[35]. *Helicobacter pylori* Ligand binding allows recruitment and oligomerization of NLRC4, which acts as an adaptor to activate caspase-1[23,38]. Both *S Typhimurium* and *S flexneri* also induce activation of the NLRC4 inflammasome independently of PKCδ[39]. However, our results support that NLRC4 phosphorylation mediated by PKCδ is necessary for NLRC4 activation.

LncRNAs are involved in numerous important biological phenomena[11,12]. We demonstrate that *LNCGM1082* can bind with PKCδ and NLRC4 to cause the phosphorylation of NLRC4. Other also found that cytoplasmic lncRNAs can participate in regulating protein stability and modification[40,41].

Methods

All reagents and oligoes used in study were listed in Supplementary Table 1.

Mice and cell lines.*LNCGM1082* deficient mice on a C57BL/6J background were generated by the Model Animal Research Center of Nanjing University (Nanjing, Jiangsu, China) using CRISPR-Cas9 system. Cas9 mRNA and sgRNA were co-injected into zygotes, sgRNA direct Cas9 endonuclease cleavage in upstream of E1 and downstream of E2, and create a DSB (double-strand break). Such breaks were repaired by non-homologous end joining (NHEJ), and resulted in deletion of Arhgap33os gene (LNCGM1082). Caspase1/11-/- and NLRC4-/- were from Prof. Shao, National Institute of Biological Sciences, Beijing; NLRP3-/- was from Prof. Meng, Pasteur Institute, shanghai; TLR5-/- was from Institute of Model Animal, Wuhan University; C57BL/6 and B6.SJL-CD45a(Ly5a) (CD45.1) mice were purchased from the Model Animal Research Center of Nanjing University (Nanjing, Jiangsu, China). All mice were maintained under specific pathogen-free (SPF) conditions in the Animal Center of Nankai University. All animal experiments were carried out in accordance with Nankai University Guide for the Care and Use of Laboratory Animals.

Human embryonic kidney cell line HEK 293T cells were obtained from the American Type Culture Collection.

Mouse models. For *S. T* infection, Salmonella infection model was performed according to the previous method[42]. Briefly, mice were withdrew from water and food for 4 hours before oral gavage treatment, and gavaged mice with 7.5 mg of streptomycin. At 20 hours after streptomycin treatment, mice were withdrawn from water and food again and then infected with S. T (200 cfu). Mice were weighed every other day for the determination of percent weight change. This was calculated as: % weight change = (weight at day X-day 0 / weight at day 0) × 100. Mice were sacrificed at the indicated days for histological study. Representative colon and lung tissues were embedded in paraffin for hematoxylin/eosin (H&E) staining, cellular flow analysis and embedded in OCT compound (Tissue-Tek, Sakura, Torrance, CA) and frozen over liquid nitrogen for immuno-staining. Lungs, liver, and spleen were collected and then

homogenized for 2 min in PBS with metal beads by using a TissueLyser II apparatus (Qiagen). CFU values were quantified by plating lysates onto LB agar, followed by incubation overnight.

For *E. coli 0160* labeled GFP infection model, mice were treated with pan-antibiotics (ampicillin (A, 1 g/L, Sigma), vancomycine (V, 0.5g/L), neomycin sulfate (N, 1 g/L), and metronidazole (M, 1g/L)) via the drinking water for one week. To confirm the elimination of bacteria, stool was collected from antibiotic-treated and untreated mice and cultured in anaerobic and aerobic condition. After confirming the elimination of bacteria, mice were gavaged using 1×10^9 CFU *E. coli*. After two days, colon and feces were collected and CFUs were quantified by plating lysates onto LB agar, followed by incubation overnight.

For chronic toxicity of LPS, mice were intraperitoneally injection with 20mg/kg LPS (O111:B4), and then serum IL1β and IL18 concentration were detected. For acute toxic experiment, mice were injected with 52mg/kg LPS (O111:B4), and then survival (time to moribund) were detected.

For bone marrow cell (BMC) transplanted experiments(BMT), BMCs collected from wt or *LNCGM1082* mice were injected into different recipient mice,which were irradiated using a Shepherd Mark I Cesium Irradiator (J.L. Shepherd and Associates) to total body irradiation at 800 cGy (a single dose). After 3 weeks, *S.T* infection was performed in these recipient mice.

Cell culture. All cells were cultured at 37°C in 95% air and 5% CO2. Peritoneal macrophages were collected by intraperitoneal injection of 2 ml BBL thioglycollate medium, brewer modified (4%; BD), and then they were recovered 4 d later by peritoneal lavage with 5 ml PBS. The peritoneal macrophages were cultured in DMEM cell culture medium (Gibco) containing 10% FBS (Gibco), 1% penicillin, and streptomycin. For bone marrow derived macrophages (BMDMs),BMDMs were obtained from bone marrow of the tibia and femur and cultured in DMEM with 10% FBS, 20 ng/ml mouse M-CSF (PeproTech), and 1% penicillin/streptomycin for 6 d and then replated and used for experiments. HEK293T cells were cultured in DMEM cell culture medium containing 10% FBS, 1% penicillin, and streptomycin.

Ex vivo stimulation. For activation of the toll-like receptors, BMDMs were stimulated with Pam3CSK4 (50nM, TLR 1/2), Poly(I:C) (10μg/ml, TLR3), LPS (2μg/ml, TLR4), flagellin (5μg/ml, TLR5), FSL-1 (50ng/ml, TLR2/6), R848(5μg/ml, TLR7/8) and ODN 1585(5μM, TLR9) for 12hrs.

For inflammasome activation, the peritoneal macrophages were primed with LPS(2μg/mL) for 4 h, and subsequently stimulated with ATP (5 mM) or nigericin (5μM) for 0.5 h to activate NLRP3 inflammasome, DOTAP-transfected flagellin (5μg/mL) for 3h to activate NLRC4 inflammasome, Lipofectamine 2000-transfected poly (dA:dT) (1μg/mL) for 3 h to activate AIM2 inflammasome. Total cell lysates and supernatants were analyzed by immunoblotting.

For *Salmonella* stimulation *in vitro*, The *S. Typhimurium* strain was grown in Luria-Bertani medium at 37°C for overnight culture. Bacteria were added to macrophages at a multiplicity of infection (MOI) of 5 for 3h, total cell lysates and precipitated supernatants were analyzed by immunoblotting.

Lentiviruses and plasmid construction. GM1082 shRNA targets were chosen from the target sequences produced by BLOCK-iT™ RNAi Designer (Invitrogen) and/or by i-Score Designer. The shRNA constructs were made using pGreenPuro™ shRNA Cloning and Expression Lentivector kit (System Biosciences Inc.) according to the manual. The control shNC is the Luciferase Control shRNA from the kit. For packaging of lenti-virus particles, the shRNA lentivector together with pMD2G and psPAX2 packaging plasmids were cotransfected into 293T cells.

For preparation of plasmids, the sequences of mouse NLRC4, including NA-LRR, LRR, ΔLRR, CARD-NA, mouse PKCδ,human NLRC4, human PKCδ and mouse/humanGM1082 were amplified using PCR methods. The PCR products were cloned into the pcDNA™3.1/V5-His TOPO® TA plasmid (Invitrogen). After sequencing, plasmid constructions were used to transfect HEK 293T.

RNA extraction and qRT-PCR. Total RNA was extracted from the cells, tissues and organs using TRIzol reagent (Invitrogen). First-strand cDNA was generated from total RNA using oligo-dT/random primer mix and reverse transcriptase (Invitrogen Corp). Quantitative real-time PCR (qRT-PCR) was conducted using QuantiTect SYBR Green PCR Master Mix (Qiagen) and specific primers in an ABI Prism 7000 analyzer (Applied Biosystems). GAPDH mRNA expression was detected in each experimental sample as an endogenous control. The fold changes were calculated using the ΔΔCt method according to the manufacturer's instructions (Applied Biosystems). All the reactions were run in triplicate.

Northern blot. For northern blot, harvested total RNAs were run on 1% agarose formaldehyde gel, and then transferred to a Hybond nylon membrane using the Trans-Blot SD semy-dry electrophorectic transfer (BioRad). Membrane was pre-hybridized for 1 hr at 42ºC and incubated with the probe overnight at the same temperature. After washing, membrane was blocked and incubated with digoxin antibody conjugated with HRP.

Western blot. For western blot, our previous method[43] was used in this study. Briefly, cells were harvested at the indicated times and rinsed twice with ice cold PBS. Cell extracts were prepared with lysis buffer and centrifuged at 13,000 g for 10 min at 4°C. Protein samples were electrophoresed using 12% polyacrylamide gels and transferred to PVDF membranes. After the membranes were blocked with 5 % Skim milk powder for 1 h at room temperature, they were incubated with first antibody in TBST overnight at 4°C. Secondary antibodies with horseradish peroxidase (HRP) (1:10000) were labeled according to our previous method. The signals were checked by autoradiography film when HRP substrate was added to the membranes.

Cytosolic and nuclear fractionation. Indicated cells were incubated with hypotonic buffer (25 mM Tris-HCl, pH 7.4, 1 mM MgCl2, 5 mM KCl) on ice for 5 min. An equal volume of hypotonic buffer containing 1% NP-40 was then added, and each sample was left on ice for another 5 min. After centrifugation at 5000 × g for 5min, the supernatant was collected as the cytosolic fraction. The pellets were resuspended in nucleus resuspension buffer (20 mM HEPES, pH 7.9, 400 mM NaCl, 1 mM EDTA, 1 mM EGTA, 1 mM DTT,

1 mM PMSF) and incubated at 4°C for 30 min. Nuclear fraction was collected after removing insoluble membrane debris by centrifugation at 12,000g for 10 min.

H & E staining. For hematoxylin/eosin (H&E) staining, previously reported methods were used in this experiment[43]. Briefly, lung tissues were fixed in 4% (w/v) paraformaldehyde buffered saline and embedded in paraffin, 5 μm sections colon sections were cut and stained with H&E.

Cell isolation and flow cytometry. For the staining of lamina propria (LP) lymphocytes, colon was isolated, cleaned by shaking in ice-cold PBS four times before tissue was cut into 1 cm pieces. The epithelial cells were removed by incubating the tissue in HBSS with 2 mM EDTA for 30 min with shaking. The LP cells were isolated by incubating the tissues in digestion buffer (DMEM, 5% fetal bovine serum, 1 mg/ ml Collagenase IV (Sigma-Aldrich) and DNase I (Sigma-Aldrich) for 40 min at 37^{o}C with shaking. The digested tissues were then filtered through a 40-mm filter. Cells were resuspended in 10 ml of the 40% fraction of a 40: 80 Percoll gradient and overlaid on 5 ml of 80% fraction in a 15 ml Falcon tube. Percoll gradient separation was performed by centrifugation for 20 min at 1,800 rpm at room temperature. LP cells were collected at the interphase of the Percoll gradient, washed and resuspended in medium, and then stained and analyzed by flow cytometry. Dead cells were eliminated through 7-AAD staining.

LNCGM1082 deletion in human macrophages. Briefly, analyze the target gene sequence, screen suitable target sites, and design one sgRNA for each target site. According to the designed sgRNA sequence, Oligo DNA was synthesized. The empty vector was digested with Cas9 gene (with fluorescent tag (GFP) and screening gene (puromycin)) to obtain linearized plasmid. Oligo DNA was mixed with linearized empty vector and ligated with T4 ligase and connected overnight at 16°C. The verified plasmid was amplified and cultured, and the plasmid was extracted. THP-1 cells were seeded in 12-well plates at a density of 100,000 cells per well. After 24 h, the cells were transiently transfected with 4 μg Cas9 plasmid using Lipofectamine 2000 (Life Technologies). After 24 h of transfection, puromycin was added with a final concentration of 3 ug to the culture dish for screening. After 3 days, the cells were diluted to a density of 1–2 cells/200 ul in 40 mL of complete growth medium, cells were plated in a 96-well plate. After 5 days, the 96-well plate was observed under an optical microscope and marked the wells containing single cells. After the cell density reaches 70%~90%, the cell genome is extracted and amplified with the previously designed PCR primers, and the amplified products are sequenced.

Immunostaining and RNA-FISH. Immunostaining and RNA fluorescence in situ hybridization (RNA-FISH) were performed according to our reported protocol[44]. Briefly, cells were first slicked on sterile and 0.01% poly-lysine-treated slides in the bottom of 6-well tissue culture dish. After that, the slides were processed sequentially with ice-cold CSK buffer, CSK + 0.4% Triton X-100 buffer and CSK buffer for 30 s for cell membrane perforation. The slides were then treated with 4% PFA for 10 min and cold 70% ethanol three times for cells fixation. After rinsed three times with ice cold PBS, the slides were blocked in pre-warmed 5% goat serum for 30 min at 37°C. Then, the slides were incubated with primary antibody at 37°C for 1 h, washed three times with 1×PBS/0.2 % Tween-20 for 3 min on a rocker, and then incubated with secondary antibody at 37°C for 30 min. The slides were dehydrated by moving them through a room

temperature ethanol series (85, 95, and 100 % ethanol) for 2 min each, and air-dried at room temperature for 15 min and hybridized using the indicated probes overnight at 37°C in a humid chamber. After washing with 2× SSC/50 % formamide, 2× SSC, and 1× SSC each for three times, DAPI dye was added. Finally, the slides were sealed, and then observed using confocal microscope.

RNA Immunoprecipitation (RIP). RNA immunoprecipitation was performed according to previously reported protocol[13]. Briefly, the cells were harvested, washed, added ice cold IP lysis buffer (Thermo Scientific Pierce) containing 0.5% ribonuclease inhibitor (Invitrogen), and incubated on ice for 5 minutes with periodic mixing. Then the lysates were transferred into a microcentrifuge tube and centrifuged at 13,000 g for 10 minutes to pellet the cell debris at 4°C, and the supernatants were transferred into a new tube, and protein G agarose was added and incubated for 1 hour at 4°C with rotation for preclearing. The immunoprecipitating antibody was added and incubated overnight at 4°C with rotation. Protein G agarose was pelleted by brief centrifugation (3000 g for 1 minute) and then washed sequentially with IP lysis buffer (containing 0.5% ribonuclease inhibitor). Finally, RNA was extracted from protein/RNA complexes on the beads using TRIzol reagent and dissolve in DEPC-water and quantified by quantitative PCR (qPCR).

UV-RIP. The cells were incubated for 12 hr with 100 mM 4-thiouridine (4-SU) and then were cross-linked using 365 nm UV light with a CL-1000 Ultraviolet Crosslinker (UVP). After lysis, cell lysates were immunoprecipitated with primary antibody or isotypic antibody. RNase T1-treated (final concentration 50 U/mL) and subsequent beads were washed with high-salt wash buffer (50 mM HEPES-KOH, pH 7.5, 500 mM KCl, 0.05% (v/v) NP40, 0.5 mM DTT, Protease Inhibitor Cocktail (Sigma-Aldrich). For UV-RIP-seq, protein-RNA complex was treated with proteinase K. Immunoprecipitated RNA was purified using acidic phenol, and RNA was subjected to high-throughput sequencing by HiSeq 4000 with PE100 strategy. For RIP-q-PCR analysis, the primers were used listed in supplemental table 1. The amount of immunoprecipitated RNAs was represented as the percentile of input RNA (% input).

Individual-nucleotide resolution cross-linking and immunoprecipitation (iCLIP). The cells were first subjected to crosslinking with 0.15 J/cm^2 of 254 nm UV light in a crosslinker HL-2000 (UVP), and then lysed with NP-40 lysis buffer on ice for 10 min and treated with RNAase A (200ng/ml) for 5 min (Promega). Clear lysates were incubated with anti-NLRC4 or isotypic antibody overnight at 4^{o}C. After immunoprecipitation, beads were left for linking biotin-labeled linker. After being separated on a 4–12% NuPAGE gel (Invitrogen NP0321B0X), the protein–RNA complexes were transferred to NC membrane. Biotin-labeled RNA was detected and visualized according to the instructions of the chemiluminescent kit (Thermo 89880). Protein–RNA complexes were cut from the membrane corresponding to the visualized size of NLRC4. RNAs were isolated from the solution with phenol-chloroform and subjected to library construction.

Immunoprecipitation. Immunoprecipitation (IP) was performed according to our previously method[13]. The cells were lysed in IP lysis buffer (Pierce) containing 10% PMSF. Protein A/G magnetic beads (Pierce) were first added into the cell lysates for preclearing. The supernatants were collected after centrifuging at

12,000 rpm and then immunoprecipitated overnight at 4°C with the indicated antibodies. Protein A/G Magnetic Beads were added into cell lysates and incubated for additional 3 hrs. After being washed with IP lysis buffer for five times, Protein A/G Magnetic Beads were denatured and resolved by SDS-PAGE gels.

RNA-protein pull-down analyses. RNA-protein pull-down analyses were performed using Pierce™ Magnetic RNA-Protein Pull-Down Kit. Transfected and induced cells were harvested and cell lysates were prepared using IP lysis buffers (Thermo Scientific Pierce).GM1082 and its mutants were transcribed (NEB, manual HiScribe T7 in vitro transcription Kit) and labeled using RNA 3´ Desthiobiotinylation Kit (Thermo Scientific Pierce) in vitro (5). 50ul beads and 50pmol of labeled RNA were added into RNA capture buffer, and incubated for 30 minutes at room temperature with agitation to binding of labeled GM1082 to streptavidin magnetic beads. After washing beads with an equal volume of 20mM Tris (pH 7.5), 100µL of protein-RNA binding buffer was added into the beads and mixed well. 100µL of master mix of RNA-protein binding reaction was added to the RNA-bound beads, mixed by pipetting and then incubated 60 minutes at 4°C with rotation to binding of RNA-binding proteins to RNA. After washing beads with 100ul wash buffer for twice, 50µL of elution buffer was added and incubated 30 minutes at 37°C with agitation. The samples were analyzed on a gel.

Isothermal titration calorimetry measurements. Calorimetric experiments were conducted at 25 ^{0}C with a MicroCal iTC200 instrument. NLRC4 and PKCδ protein was dialyzed against the titration buffer containing 20 mM Tris-HCL, pH 7.4, 150 mM NaCl, and 2 mM $MgCl_2$. Lyophilized RNA samples were prepared in the titration buffer, renatured at 95^{o}C for 2min, 4^{o}C for 2min and 25°Cfor 20min, and then diluted to be required concentration for isothermal titration calorimetry (ITC) titration. Acquired calorimetric titration data were analyzed using software origin 7.0 based on the ‘One Set of Sites’ fitting model.

Statistical Analyses. Two side Student's t-test and ONE-way ANOVA Bonferroni’s Multiple Comparison Test were used to determine significance. The statistical significance of the survival curves was estimated using Kaplan and Meier method, and the curves were compared using the generalized Wilcoxon's test. These were performed by GraphPad Prism 5 software (GraphPad Software). A 95% confidence interval was considered significant and was defined as $p < 0.05$.

Data Availability

The accession number for the RNA-seq data reported in this paper is NCBI GEO: https://www.ncbi.nlm.nih.gov/geo/query/acc.cgi?acc=GSE173401

Declarations

Author contributions

R.Y. designed the research and wrote the paper; Y. G. conducted *in vivo* and *in vitro* experiments for mechanisms; Y.Y., Q. Z. mainly conducted *in vivo* experiments and immunoassays; J. W., J. Y., Y. W., M. J.,

R. W., X. Y. performed partly *in vitro* experiments; J. Z., X. L offered an assistant for ITC analyses; Y. Z. offered assistance for the animal experiments. All authors read and approved the final manuscript.

Acknowledgements

This research was supported by NSFC grants (grant number 91842302, 81970457, 81901677 and 91629102); The Tianjin Science and Technology Commission (grant number, 18JCZDJC35300); A Ministry of Science and Technology (grant number, 2016YFC1303604); The State Key Laboratory of Medicinal Chemical Biology and the Fundamental Research Funds for the Central University, Nankai university (63191724).

Competing interests

The authors declare no conflict of interest.

Conflicts of interest

Authors disclose no conflict

References

1. Kay, C., Wang, R., Kirkby, M. & Man, S. M. Molecular mechanisms activating the NAIP-NLRC4 inflammasome: Implications in infectious disease, autoinflammation, and cancer. *Immunol Rev* **297**, 67-82 (2020).
2. Duncan, J. A. & Canna, S. W. The NLRC4 Inflammasome. *Immunol Rev* **281**, 115-123 (2018).
3. Lamkanfı, M. & Dixit, V. M. Mechanisms and functions of inflammasomes. *Cell* **157**, 1013-1022 (2014).
4. Rathinam, V. A. & Fitzgerald, K. A. Inflammasome Complexes: Emerging Mechanisms and Effector Functions. *Cell* **165**, 792-800 (2016).
5. Zhao, Y. et al. The NLRC4 inflammasome receptors for bacterial flagellin and type III secretion apparatus. *Nature* **477**, 596-600 (2011).
6. Zhao, Y. & Shao, F. The NAIP-NLRC4 inflammasome in innate immune detection of bacterial flagellin and type III secretion apparatus. *Immunol Rev* **265**, 85-102 (2015).
7. Qu, Y. et al. Phosphorylation of NLRC4 is critical for inflammasome activation. *Nature* **490**, 539-542 (2012).
8. Liu, W. et al. LRRK2 promotes the activation of NLRC4 inflammasome during Salmonella Typhimurium infection. *J Exp Med* **214**, 3051-3066 (2017).

9. Raghawan, A. K. et al. A Disease-associated Mutant of NLRC4 Shows Enhanced Interaction with SUG1 Leading to Constitutive FADD-dependent Caspase-8 Activation and Cell Death. *J Biol Chem* **292**, 1218-1230 (2017).
10. Esteller, M. Non-coding RNAs in human disease. *Nat Rev Genet* **12**, 861-874 (2011).
11. Rinn, J. L. & Chang, H. Y. Genome regulation by long noncoding RNAs. *Annu Rev Biochem* **81**, 145-166 (2012).
12. Ponting, C. P., Oliver, P. L. & Reik, W. Evolution and functions of long noncoding RNAs. *Cell* **136**, 629-641 (2009).
13. Gao, Y. et al. Lnc-C/EBPbeta Negatively Regulates the Suppressive Function of Myeloid-Derived Suppressor Cells. *Cancer Immunol Res* **6**, 1352-1363 (2018).
14. Zhang, P., Cao, L., Zhou, R., Yang, X. & Wu, M. The lncRNA Neat1 promotes activation of inflammasomes in macrophages. *Nature communications* **10**, 1495 (2019).
15. Broz, P. & Dixit, V. M. Inflammasomes: mechanism of assembly, regulation and signalling. *Nat Rev Immunol* **16**, 407-420 (2016).
16. Mariathasan, S. et al. Cryopyrin activates the inflammasome in response to toxins and ATP. *Nature* **440**, 228-232 (2006).
17. Rathinam, V. A. K., Zhao, Y. & Shao, F. Innate immunity to intracellular LPS. *Nat Immunol* **20**, 527-533 (2019).
18. Sharif, H. et al. Structural mechanism for NEK7-licensed activation of NLRP3 inflammasome. *Nature* **570**, 338-343 (2019).
19. Zhang, Z. et al. The helicase DDX41 senses intracellular DNA mediated by the adaptor STING in dendritic cells. *Nat Immunol* **12**, 959-965 (2011).
20. Amer, A. et al. Regulation of Legionella phagosome maturation and infection through flagellin and host Ipaf. *J Biol Chem* **281**, 35217-35223 (2006).
21. Man, S. M. Inflammasomes in the gastrointestinal tract: infection, cancer and gut microbiota homeostasis. *Nat Rev Gastroenterol Hepatol* **15**, 721-737 (2018).
22. Man, S. M. et al. Inflammasome activation causes dual recruitment of NLRC4 and NLRP3 to the same macromolecular complex. *Proc Natl Acad Sci U S A* **111**, 7403-7408 (2014).
23. Rauch, I. et al. NAIP-NLRC4 Inflammasomes Coordinate Intestinal Epithelial Cell Expulsion with Eicosanoid and IL-18 Release via Activation of Caspase-1 and -8. *Immunity* **46**, 649-659 (2017).
24. Sellin, M. E. et al. Epithelium-intrinsic NAIP/NLRC4 inflammasome drives infected enterocyte expulsion to restrict Salmonella replication in the intestinal mucosa. *Cell Host Microbe* **16**, 237-248 (2014).
25. Han, X., Ding, S., Jiang, H. & Liu, G. Roles of Macrophages in the Development and Treatment of Gut Inflammation. *Frontiers in cell and developmental biology* **9**, 625423 (2021).
26. Perkins, D. J. et al. Salmonella Typhimurium Co-Opts the Host Type I IFN System To Restrict Macrophage Innate Immune Transcriptional Responses Selectively. *Journal of immunology* **195**,

2461-2471 (2015).
27. Qi, H. et al. Reg4 and complement factor D prevent the overgrowth of E. coli in the mouse gut. *Commun Biol* **3**, 483 (2020).
28. Gram, A. M. et al. Salmonella Flagellin Activates NAIP/NLRC4 and Canonical NLRP3 Inflammasomes in Human Macrophages. *Journal of immunology* **206**, 631-640 (2021).
29. Reyes Ruiz, V. M. et al. Broad detection of bacterial type III secretion system and flagellin proteins by the human NAIP/NLRC4 inflammasome. *Proceedings of the National Academy of Sciences of the United States of America* **114**, 13242-13247 (2017).
30. Smith, K. D. et al. Toll-like receptor 5 recognizes a conserved site on flagellin required for protofilament formation and bacterial motility. *Nat Immunol* **4**, 1247-1253 (2003).
31. Miao, E. A. et al. Cytoplasmic flagellin activates caspase-1 and secretion of interleukin 1beta via Ipaf. *Nat Immunol* **7**, 569-575 (2006).
32. Ghoneim, H. E., Thomas, P. G. & McCullers, J. A. Depletion of alveolar macrophages during influenza infection facilitates bacterial superinfections. *Journal of immunology* **191**, 1250-1259 (2013).
33. Kofoed, E. M. & Vance, R. E. Innate immune recognition of bacterial ligands by NAIPs determines inflammasome specificity. *Nature* **477**, 592-595 (2011).
34. Karki, R. et al. IRF8 Regulates Transcription of Naips for NLRC4 Inflammasome Activation. *Cell* **173**, 920-933 e913 (2018).
35. Qu, Y. et al. NLRP3 recruitment by NLRC4 during Salmonella infection. *J Exp Med* **213**, 877-885 (2016).
36. Hu, Z. et al. Structural and biochemical basis for induced self-propagation of NLRC4. *Science* **350**, 399-404 (2015).
37. Zhang, L. et al. Cryo-EM structure of the activated NAIP2-NLRC4 inflammasome reveals nucleated polymerization. *Science* **350**, 404-409 (2015).
38. Hu, M. et al. [Inflammasome responses in macrophages induced by C-terminal peptides of Escherichia coli EscI protein]. *Wei Sheng Wu Xue Bao* **55**, 1350-1355 (2015).
39. Suzuki, S. et al. Shigella type III secretion protein MxiI is recognized by Naip2 to induce Nlrc4 inflammasome activation independently of Pkcdelta. *PLoS pathogens* **10**, e1003926 (2014).
40. Wang, P. et al. The STAT3-binding long noncoding RNA lnc-DC controls human dendritic cell differentiation. *Science* **344**, 310-313 (2014).
41. Li, Z. et al. The LINC01138 drives malignancies via activating arginine methyltransferase 5 in hepatocellular carcinoma. *Nature communications* **9**, 1572 (2018).
42. Cao, S. et al. The Gut Epithelial Receptor LRRC19 Promotes the Recruitment of Immune Cells and Gut Inflammation. *Cell Rep* **14**, 695-707 (2016).
43. Su, X. et al. LRRC19 expressed in the kidney induces TRAF2/6-mediated signals to prevent infection by uropathogenic bacteria. *Nat Commun* **5**, 4434 (2014).

44. Shang, W., Gao, Y., Tang, Z., Zhang, Y. & Yang, R. The Pseudogene Olfr29-ps1 Promotes the Suppressive Function and Differentiation of Monocytic MDSCs. *Cancer Immunol Res* **7**, 813-827 (2019).

Figures

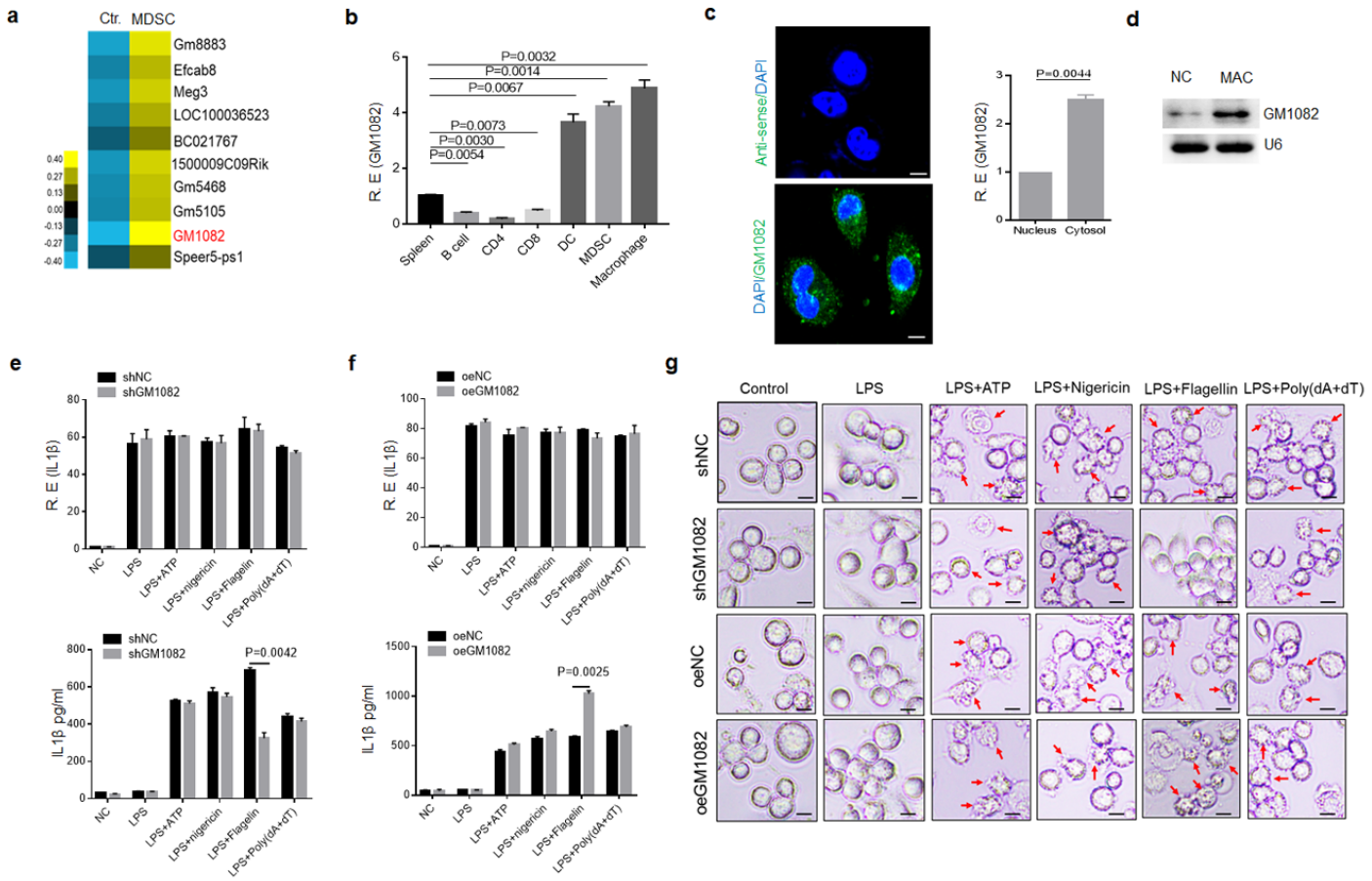

Figure 1

LncGM1082 enhances IL-1β maturation and pyroptosis in macrophages. a. LncRNA microarray of myeloid derived suppressor cells (MDSCs). MDSCs were generated, and lncRNA expression was then evaluated using an lncRNA expression microarray. Ctr., bone marrow cells. b. QRT-PCR of LNCGM1082 in spleen, B cell, CD4, CD8, dendritic cells (DC), MDSC and macrophages sorted from spleen by flow cytometry. R. E, relative expression. c. Fluorescence in situ hybridization of LNCGM1082 in mouse macrophage and QRT-PCR analysis of LNCGM1082 in the cytosol and nucleus. Nuclei were stained with DAPI (blue); Green, LNCGM1082. Scale bar, 2.5 μM. d. Northern blot of murine LNCGM1082 in mouse macrophages. NC, Bone marrow cells; MAC, macrophages. e-f. QRT-PCR of IL-1β and ELISA analysis of IL-1β in the supernatatnts of wt, LNCGM1082 shRNA (shGM1082) and exogenous LNCGM1082 (oeGM1082) transfected macrophages, which were stimulated by different stimulators. R. E, relative expression. g. Images of the LNCGM1082 shRNA (shGM1082) and exogenous LNCGM1082 (oeGM1082)

transfected macrophages under light microscopy after stimulated by LPS plus ATP, LPS plus nigericin, LPS plus flagellin and LPS plus poly(dA+dT). Scale bar, 5 μM. The arrows indicate pyroptotic cells. Student's t-test in b, c, e and f, mean ±SD.

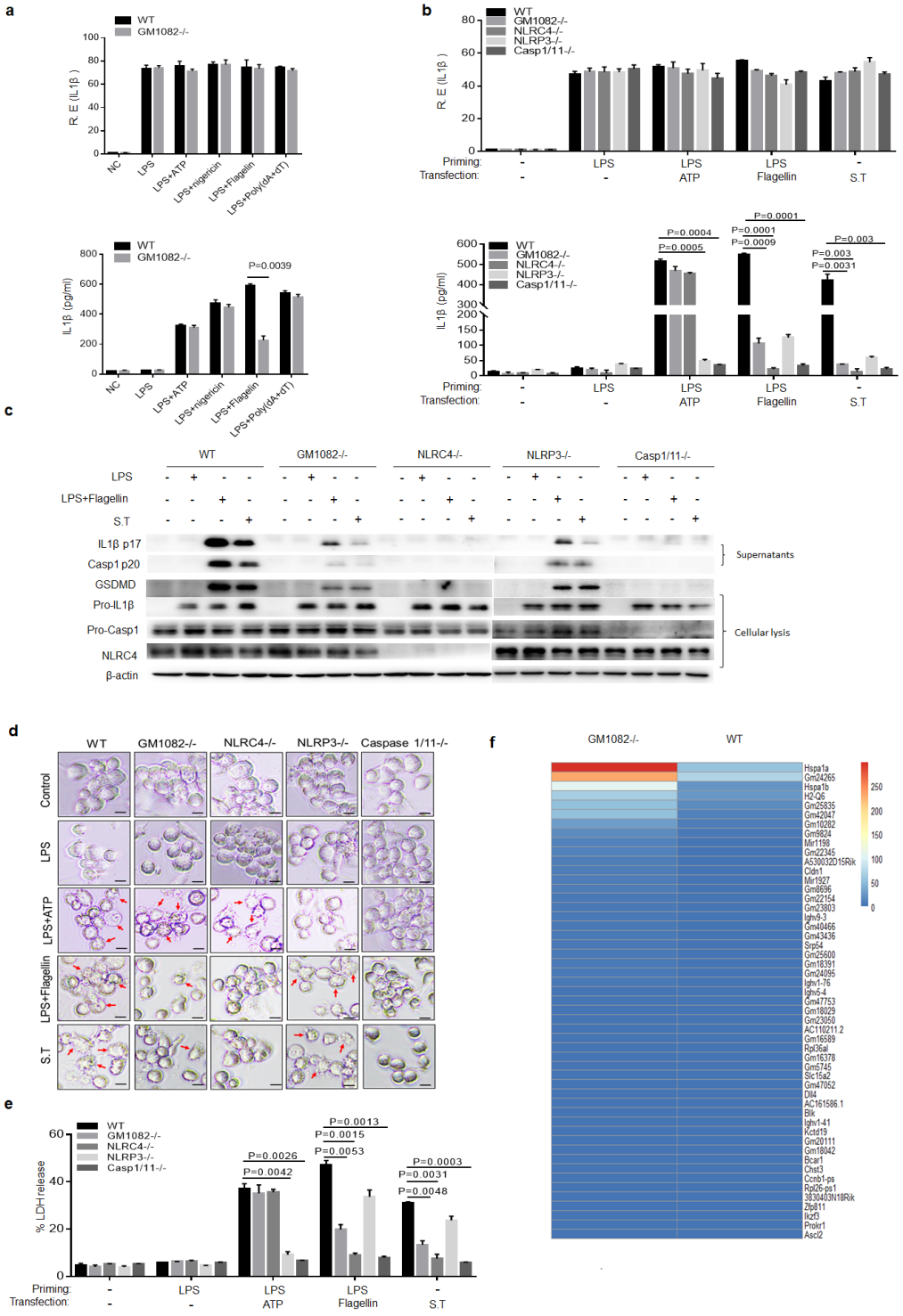

Figure 2

LNCGM1082-/- macrophages are similar with NLRC4-/- macrophages in the IL-1β maturation and pyroptosis. a. QRT-PCR of IL-1β and ELISA of IL-1β in the supernatants of wt and LNCGM1082-/-

macrophages, which were stimulated by different stimulators. R. E, relative expression. b. QRT-PCR of IL-1β and ELISA of IL-1β in the supernatants of wt, LNCGM1082-/-, NLRC4-/-, NLRP3-/- and caspase-1/11-/- macrophages, which were stimulated by LPS plus ATP, LPS plus flagellin or infected by S. T. R. E, relative expression. c. Western blots of the macrophages and their supernatants, which were stimulated by LPS plus flagellin or S. T. d. Images of the macrophages under light microscopy after stimulated by LPS plus ATP, LPS plus flagellin or S. T. The arrows indicate pyroptotic cells. Scale bar, 5 μM. e. LDH in the supernatants of the macrophages, which were stimulated by LPS plus ATP, LPS plus flagellin or S. T.. f. Microarray of wt and LNCGM1082-/- macrophages. Wt and LNCGM1082-/- bone marrow cells were exposed to M-CSF for 5days, and mRNA expression was evaluated using microarray. Student's t-test in a, b, and e, mean ±SD.

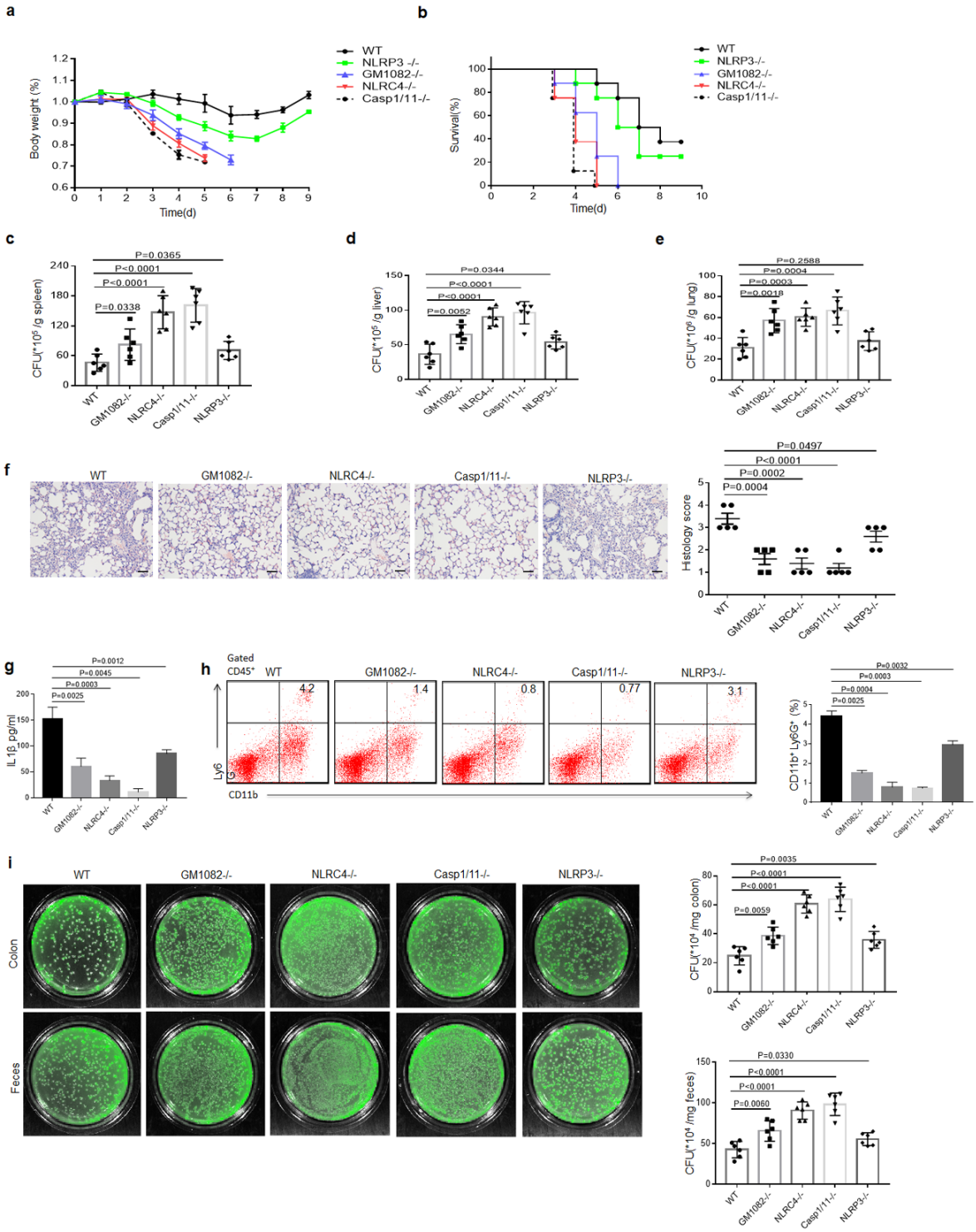

Figure 3

LNCGM1082-/-mice are similar sensitive to S. T with NLRC4-/- mice. a. Body weight of wt, LNCGM1082-/-, NLRC4-/-, NLRP3-/- and Caspase-1/11-/- mice after S. T infection. b. Survival rate of wt, LNCGM1082-/-, NLRC4-/-, NLRP3-/- and caspase-1/11-/- mice after S. T infection. c-e. CFUs in the spleen (c), liver (d) and lung (e) of wt, LNCGM1082-/-, NLRC4-/-, NLRP3-/- and caspase-1/11-/- mice after S. T infection. f. H&E staining of lung sections from the mice in (a). Scale bar, 80 μm. g. ELISA of IL-1β in the blood collected

from mice in (a). h. Flow cytometry of neutrophils (CD11b+ Ly6G+) from intestinal lamina propria of mice in (a). % CD11b+ Ly6G+ neutrophils were compared (n=5). i. Bacterial burden in the colon and feces of wt, LNCGM1082-/-, NLRC4-/-, NLRP3-/- and caspase-1/11-/- mice after GFP-labelled Escherichia coli O160 infection. Analysis of variance test in a; Wilcoxon's test in b; Two side Student's t-test in c-i.

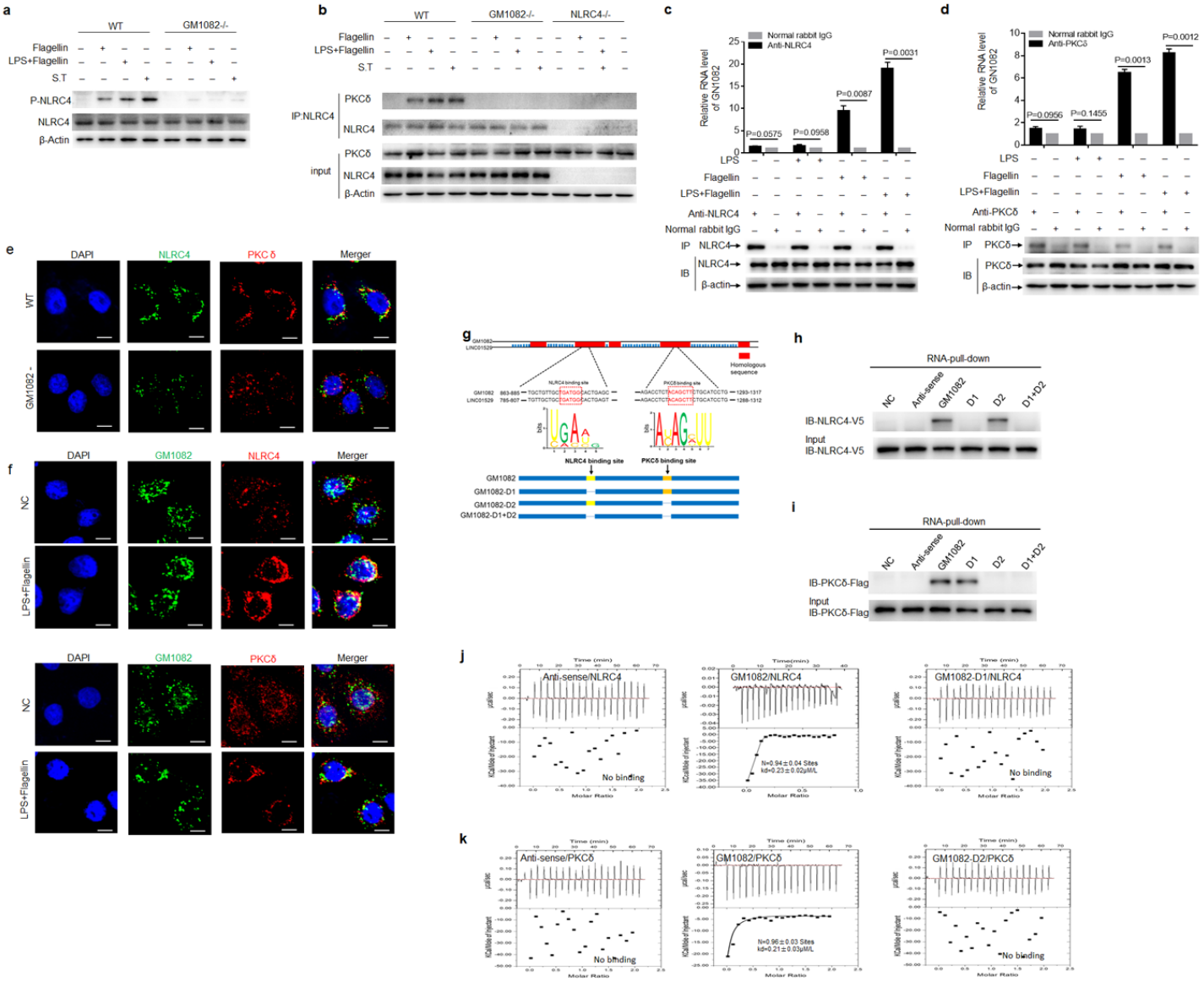

Figure 4

Binding of LNCGM1082 with NLRC4 and PKCδ to induce NLRC4 phosphorylation. a. Immunoblots of phosphorylated NLRC4 in the macrophages after exposed to S.T or flagellin. b. Immunoblot of NLRC4 and PKCσ in the macrophages. Immunoprecipitation was performed using NLRC4 antibodies, and then immunoblot using anti-PKCδ. c and d. RIP in the macrophages after exposed to flagellin or S.T. Cell lysates were incubated with normal rabbit IgG, NLRC4 and PKCδ antibody. The immunoprecipitates were analyzed by qRT-PCR to exam enrichment efficiency of LNCGM1082. e. Immunostaining of NLRC4 and PKCδ in wt and LNCGM1082-/- macrophages. Red, NLRC4; Green, PKCδ. Blue, nuclei. Scale bar, 2.5 μM. f. Immunostaining and RNA-FISH of NLRC4, PKCδ and LNCGM1082 in the macrophages. Red, NLRC4,

PKCδ; Green, LNCGM1082; Blue, nuclei. Scale bar, 2.5 μM. g. Construction of LNCGM1082 plasmids (pCDNA3.1) which lack D1, D2 and D1 + D2 sites. We used NCBI database to perform sequence comparison to find out homologous sequences and used MEME software (https://meme-suite.org/meme/) to analyze the NLRC4 and PKCδ protein binding motif. NLRC4 or PKCδ binding sites were named as “D1” or “D2”. LNCGM1082 plasmids which lack D1, D2 or D1 + D2 sites were constructed. h-i. RNA-pull down using biotinylated LNCGM1082 and LNCGM1082 fragments in V5- tagged NLRC4 or flag-tagged PKCδ transfected HEK293T cells. NC, no biotinylated LNCGM1082 and fragments. j-k. ITC analysis of the binding of mouse LNCGM1082 and mutated LNCGM1082 (deleted D1 or D2) to NLRC4 and PKCδ. Two side Student’s t-test in c and d.

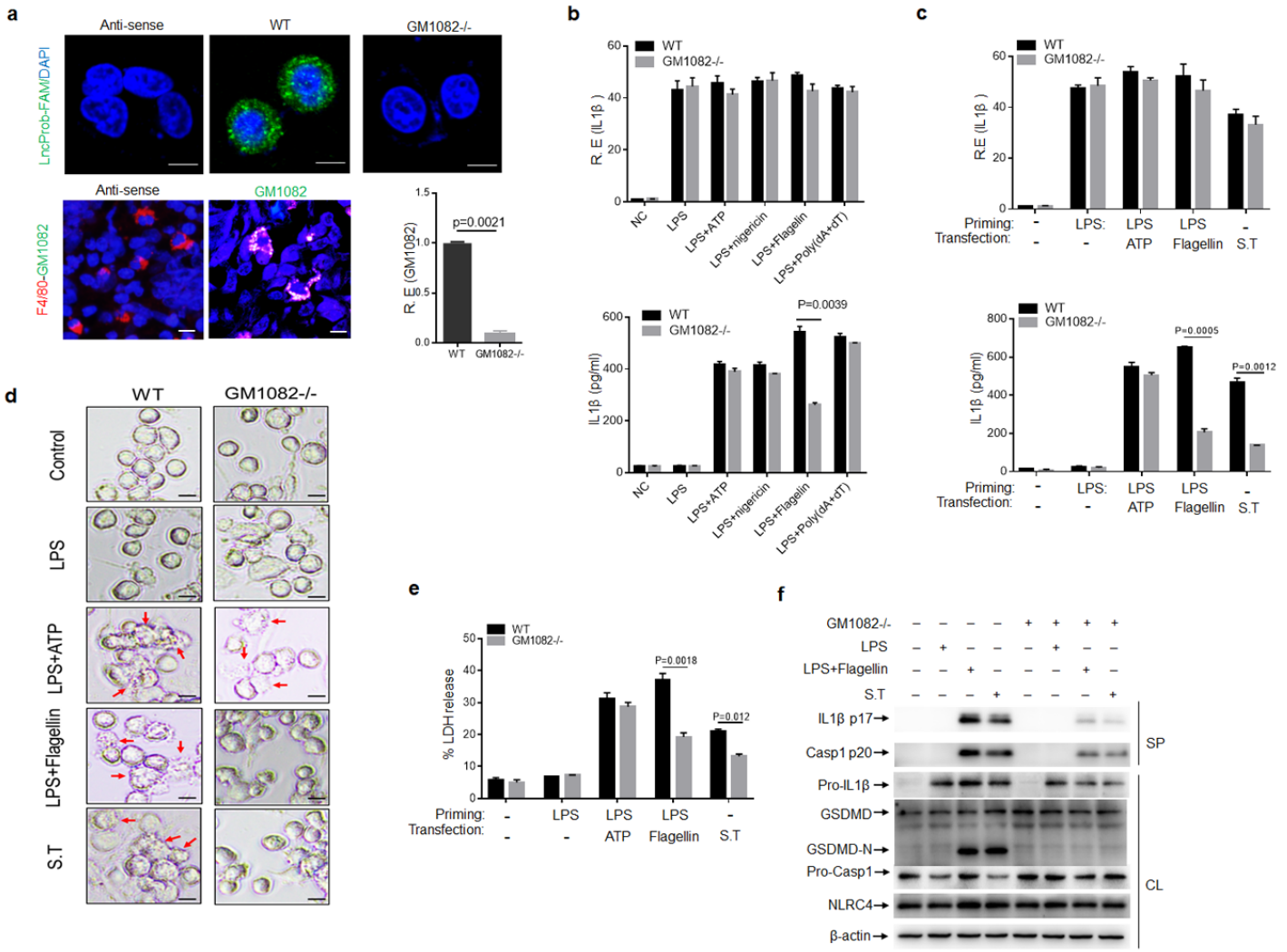

Figure 5

LNCGM1082 in human macrophages exerts similar role with mice. a. Fluorescence in situ hybridization of LNCGM1082 in monocyte/macrophage THP-1 cell line, qRT-PCR of LNCGM1082-/- THP-1 (upper) and macrophages in human colon tissues (lower). Red, F4/80; Green, LNCGM1082. Blue, nuclei. Scale bar, 2.5 μM. GM1082-/-, LNCGM1082-/- macrophages. b. QRT-PCR of IL-1β and ELISA of IL-1β in the supernatants of wt and LNCGM1082-/- THP-1 cells, which were stimulated by different stimulators. R. E, relative

expression. c. QRT-PCR of IL-1β and ELISA of IL-1β in the supernatants of wt and LNCGM1082-/- THP-1 cells, which were stimulated by LPS plus ATP, flagellin or S. T. R. E, relative expression. d. Images of THP-1 and LNCGM1082-/- THP-1 cells under light microscopy after stimulated by LPS plus ATP, LPS plus flagellin or S. T. The arrows indicate pyroptotic cells. Scale bar, 5 μM. e. LDH in the supernatants of THP-1, which were stimulated by LPS plus ATP, LPS plus flagellin or S. T. f. Western blots of THP-1 lyses and the supernatants, which were stimulated by LPS plus flagellin or S. T. SP, supernatants; CL, cell lyses. Two side Student's t-test in b, c and e.

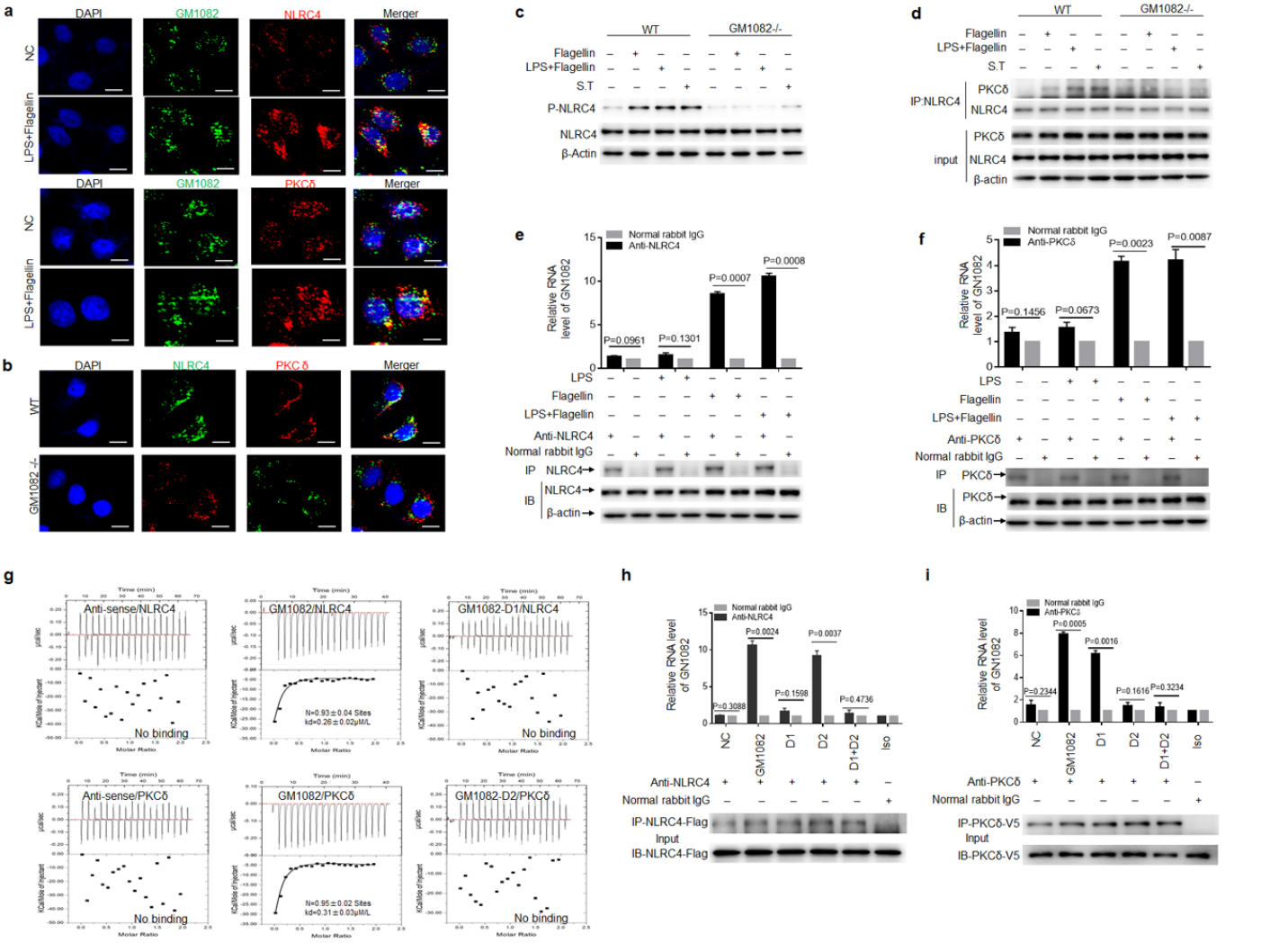

Figure 6

Binding of human LNCGM1082 with NLRC4 and PKCδ. a. Immunostaining and RNA-FISH of NLRC4, PKCδ and LNCGM1082 in THP-1 cells. Red, NLRC4, PKCδ; Green, LNCGM1082; Blue, nuclei. Scale bar, 2.5 μM. b. Immunostaining of NLRC4 and PKCδ in WT and LNCGM1082 KO THP-1 cells. Red, NLRC4; Green, PKCδ. Blue, nuclei. Scale bar, 2.5 μM. c. Western blots of NLRC4 phosphorylation in THP-1 cells after exposed to S.T or flagellin. d. Immunoblot of NLRC4 and PKCδ in THP-1 cells. Immunoprecipitation was performed using NLRC4 antibodies, and then immunoblot by anti-PKCδ. e-f. RIP in THP-1 cells after

exposed to flagellin or S.T. Cell lysates were incubated with normal rabbit IgG, NLRC4 and PKCδ antibody. The immunoprecipitates were analyzed by qRT-PCR to exam enrichment efficiency of LNCGM1082. g. ITC of the binding of human LNCGM1082 or mutated LNCGM1082 (deleted the binding site D1 of NLRC4 or D2 of PKCδ) to NLRC4 and PKCδ. h. RIP in Flag-tagged NLRC4 and LNCGM1082, LNCGM1082D1, LNCGM1082D2 or LNCGM1082D1/D2 cotransfected HEK293T cells. RIP was performed using anti-Flag antibody or control isotypic control (Iso). i. RIP in V5-tagged PKCδ and LNCGM1082, LNCGM1082D1, LNCGM1082D2 or LNCGM1082D1/D2 cotransfected HEK293T cells. RIP was performed using anti-V5 antibody or control isotypic control (Iso). Two side Student's t-test in e, f, h and i.

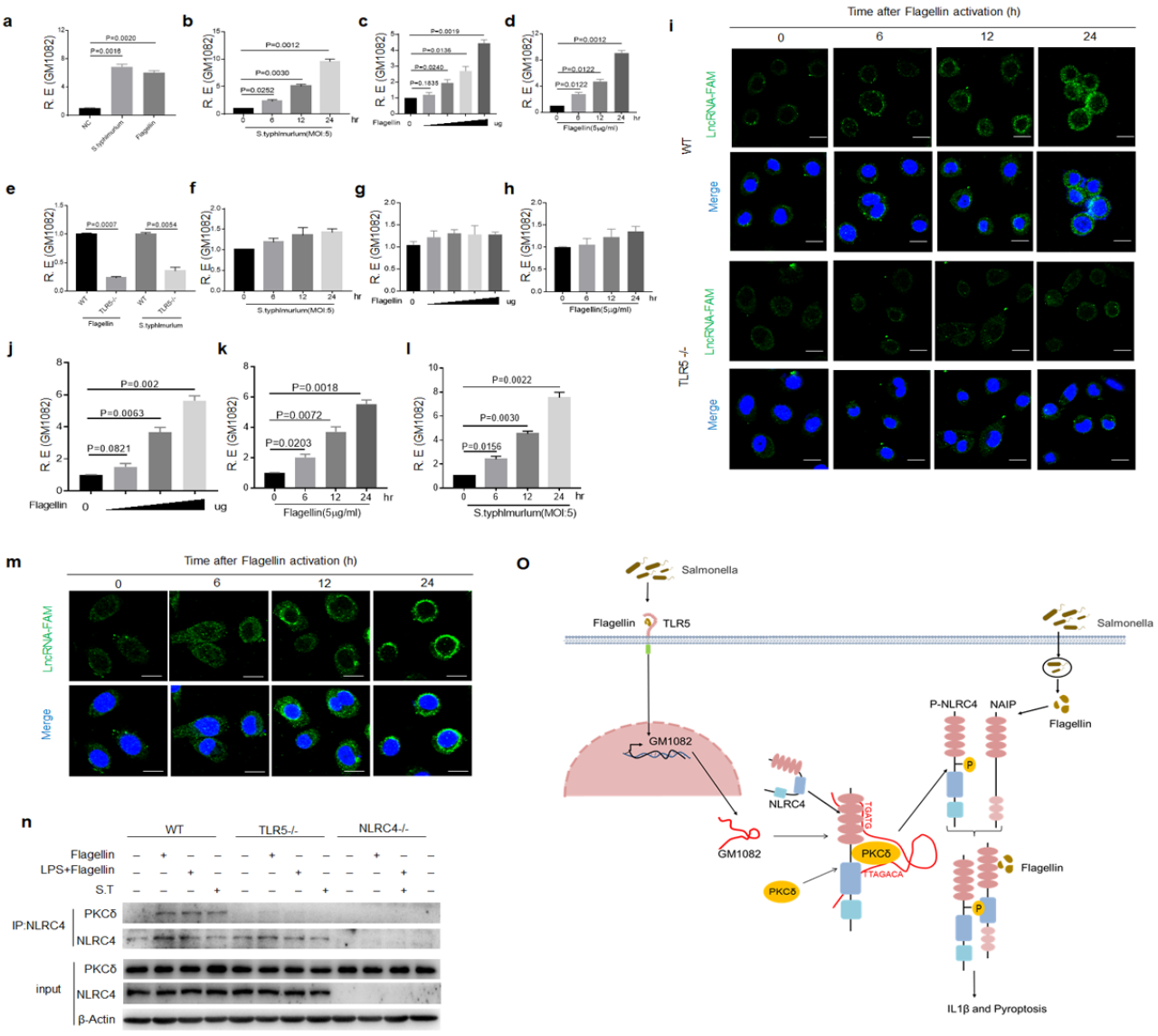

Figure 7

Flagellin induces LNCGM1082 through TLR5 in macrophages. a. QRT-PCR of LNCGM1082 in the macrophages, which were stimulated by flagellin or S. T. b. QRT-PCR of LNCGM1082 in the macrophages after exposed to S.T at different time points. c. QRT-PCR of LNCGM1082 in the macrophages after exposed to different concentration of flagellin. d. QRT-PCR of LNCGM1082 in the macrophages after exposed to flagellin at different time points. e. QRT-PCR of LNCGM1082 in WT and TLR5-/- macrophages

after exposed to flagellin or S.T. f. QRT-PCR of LNCGM1082 in TLR5-/- macrophages after exposed to S.T at different time points. g. QRT-PCR of LNCGM1082 in TLR5-/- macrophages after exposed to different concentration of flagellin. h. QRT-PCR of LNCGM1082 in TLR5-/- macrophages after exposed to flagellin at different time points. i. RNA-FISH of LNCGM1082 in WT and TLR5-/- macrophages after exposed to flagellin at different times. Green, LNCGM1082; Blue, nuclei. Scale bar, 2.5 μM. j. QRT-PCR of LNCGM1082 in THP-1cells after exposed to different concentration of flagellin. k. QRT-PCR of LNCGM1082 in THP-1 cells after exposed to flagellin at different time points. l. QRT-PCR of LNCGM1082 in THP-1 cells after exposed to S.T. at different times. m. RNA-FISH of LNCGM1082 in THP-1 cells after exposed to flagellin at different times. Green, LNCGM1082; Blue, nuclei. Scale bar, 2.5 μM. n. Immunoblot of NLRC4 and PKCδ in WT, TLR5-/- and NLRC4-/- macrophages. Immunoprecipitation was performed using NLRC4 antibodies, and then immunoblot using anti-PKCδ. o. Mechanism of LNCGM1082 induced by S.T to regulate activation of NLRC4. R. E, relative expression. Two side Student's t-test in a-h, j-i.

Supplementary Files

This is a list of supplementary files associated with this preprint. Click to download.

- Supplementaryinformation.docx